Current-induced instability of a composite free layer with antiferromagnetic interlayer coupling

Pavel Baláž* and Józef Barnaś

A. Mickiewicz University, Faculty of Physics, Umultowska 85, 61-614 Poznań, Poland
and Institute of Molecular Physics, Polish Academy of Sciences, Smoluchodwskiego 17, 60-179 Poznań, Poland

(Received 18 January 2013; revised manuscript received 8 May 2013; published 8 July 2013)

Stability conditions for a spin valve with a composite free layer consisting of two antiferromagnetically coupled films—known as synthetic antiferromagnet or ferrimagnet—is studied theoretically by means of the linearized coupled Landau-Lifshitz-Gilbert equations. The Lyapunov and Routh-Hurwitz methods have been used to examine stability of the free layer subject to external in-plane magnetic field and electric current flowing perpendicularly to the layers' plane. A simple formula for the critical current density, valid for a variety of composite free layer structures, also has been derived. The analytical results are compared with those obtained from numerical simulations in which we took into account the spin transfer torque in the diffusive spin-dependent transport model. An excellent agreement between the analytical and numerical results has been achieved.

DOI: 10.1103/PhysRevB.88.014406 PACS number(s): 72.25.Ba, 73.43.Qt, 75.47.De

I. INTRODUCTION

The physics of current-induced magnetic switching and excitations in spin valves with one reference (fixed) and one sensing (free) layers is already well understood. The driving force responsible for the magnetic dynamics is the spin torque, which is a result of spin angular momentum transfer between conduction electrons (current) and local magnetization. The current-induced magnetization dynamics of the sensing layer can be described by the Landau-Lifshitz-Gilbert (LLG) equation[1] with the spin transfer torque (STT) included.[2,3] It has been shown in many experimental[4,5] and theoretical[6–8] studies, that this equation of motion provides a proper framework for studying the current-induced magnetization dynamics in metallic spin valves as well as in magnetic tunnel junctions.[9] Additionally, it has been shown that the linearized LLG equation in static magnetic configurations can provide useful information on the magnetization stability and critical current density required for exciting the magnetization dynamics.[10–12] In the case of a simple sensing layer (a single uniform magnetic film), the critical current can be determined from the signs of trace and determinant of the corresponding 2×2 dynamic matrix.[10,13] This, however, does not apply to the case of a composite free layer (CFL). The CFL is a sensing layer which consists of two or more magnetic films separated by thin nonmagnetic layers. The adjacent magnetic layers are usually coupled ferromagnetically or antiferromagnetically due to the interlayer exchange coupling of the Ruderman-Kittel-Kasuya-Yosida (RKKY) type.[14,15] The coupled spin dynamics of the CFL enlarges dimensionality of the dynamic matrix and therefore complicates the stability analysis of the relevant static states.

In this paper we consider stability conditions for CFLs, and focus on a CFL consisting of two magnetic films with antiferromagnetic interlayer coupling. When both magnetic films are equally thick, such a CFL is called synthetic antiferromagnet (SyAF), otherwise, it is called a synthetic ferrimagnet (SyF). Current-induced switching and stability of a SyAF/SyF free layer was demonstrated experimentally[16,17] as well as studied theoretically.[18–20] In our previous numerical analysis of the current-induced dynamics of CFL structures,[21] we pointed out a nonlinear variation of the critical current density with applied magnetic field. We have also shown that the analysis of a single spin stability is not sufficient to describe the most important features of the current-induced dynamics. Thus, the present paper is a continuation of our earlier work. The main objective of this paper is to properly establish the stability conditions for the static states of a CFL, and find an appropriate description of the critical current density. Therefore, we linearize the coupled LLG equations around the in-plane static configurations of the CFL. This leads to four coupled ordinary differential equations of first order for the macrospin excitations. Then, we employ the Lyapunov theorem of stability.[22] Making use of the Routh-Hurwitz method,[23] we formulate the stability conditions for the CFL, which allows us to study the critical current density. Comparing the analytical results with numerical simulations, we show that the model based on the linearized LLG equation gives appropriate results for the critical current density in the whole range of the considered parameters. In this paper we restricted our considerations to relatively small external magnetic fields which do not destroy the equilibrium antiparallel configuration of CFLs. Moreover, in order to describe the spin transfer torque in the spin valve, we assume the model of diffusive spin-dependent electronic transport, as described in Refs. 13 and 24.

The paper is organized as follows. In Sec. II we introduce the model of current-induced dynamics of the CFL, and derive the linearized LLG equation for two coupled magnetizations. This section also describes the methods used to study stability of the static configurations of the CFL. The results are presented and accounted for in Sec. III. Summary and concluding remarks are given in Sec. IV. Additional information can be found in the Appendix.

II. THEORETICAL FORMULATION

A. Model

We consider a spin valve structure AF/F_0/N_0/CFL, shown in Fig. 1, where AF is an antiferromagnetic layer used to bias magnetization of the reference magnetic layer F_0,[25] and N_0 is the nonmagnetic spacer. In turn, CFL stands for the composite free layer F_1/N/F_2.

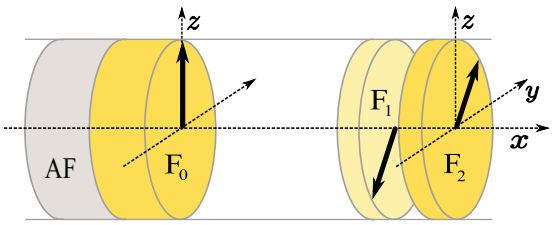

FIG. 1. (Color online) Scheme of the studied spin valve with a composite free layer F_1/N/F_2.

In the macrospin approximation, the magnetization dynamics of the CFL is described by two coupled LLG equations,

$$\frac{d\hat{\mathbf{S}}_i}{dt} + \alpha\,\hat{\mathbf{S}}_i \times \frac{d\hat{\mathbf{S}}_i}{dt} = \boldsymbol{\Gamma}_i\,,$$
$$\boldsymbol{\Gamma}_i = -|\gamma_g|\mu_0 \hat{\mathbf{S}}_i \times \mathbf{H}_{\mathrm{eff}\,i} + \frac{|\gamma_g|}{M_s d_i}\,\boldsymbol{\tau}_i\,, \quad (1)$$

for $i = 1,2$, where $\hat{\mathbf{S}}_i$ stands for a unit vector along the net spin moment of the ith layer, while $\mathbf{H}_{\mathrm{eff}\,i}$ and $\boldsymbol{\tau}_i$ are the effective magnetic field and current-induced spin torque, respectively, both acting on $\hat{\mathbf{S}}_i$. The damping parameter α, and the saturation magnetization M_s, are assumed the same for both magnetic components of the CFL. Furthermore, γ_g is the gyromagnetic ratio, μ_0 is the vacuum permeability, and d_i stands for the thickness of the F_i layer.

The effective magnetic field for the F_i layer is

$$\mathbf{H}_{\mathrm{eff}\,i} = -H_{\mathrm{app}}\,\hat{\boldsymbol{e}}_z - H_{\mathrm{ani}}(\hat{\mathbf{S}}_i \cdot \hat{\boldsymbol{e}}_z)\,\hat{\boldsymbol{e}}_z + \mathbf{H}_{\mathrm{dem}\,i} + H_{\mathrm{RKKY}\,i}\,\hat{\mathbf{S}}_j, \quad (2)$$

where $i,j = 1,2$ and $i \neq j$. In the latter equation, H_{app} is the external magnetic field applied in the layers' plane and along the easy axis (oriented opposite to the axis z), H_{ani} is the uniaxial anisotropy field (the same for both magnetic layers), and $\mathbf{H}_{\mathrm{dem}\,i} = (H^{\mathrm{d}}_{ix}S_{ix}, H^{\mathrm{d}}_{iy}S_{iy}, H^{\mathrm{d}}_{iz}S_{iz})$ is the self-demagnetization field of the F_i layer. In the calculations and simulations described below, the demagnetization fields have been calculated numerically by means of the generalized demagnetizing tensor formalism introduced by Newell *et al.*[26] For simplicity, the magnetostatic interaction between the magnetic layers has been disregarded here. This interaction, however, can be easily added to the effective field, making use of the generalized demagnetizing tensor formalism.[21,26] The influence of the magnetostatic interlayer coupling on the critical current density shall be discussed in the summary. Finally, $H_{\mathrm{RKKY}\,i}$ stands for the RKKY exchange field acting on $\hat{\mathbf{S}}_i$, which is related to the RKKY coupling constant J_{RKKY} as $H_{\mathrm{RKKY}\,i} = -J_{\mathrm{RKKY}}/(\mu_0 M_s d_i)$.[27]

Generally, the torques induced by spin polarized current flowing perpendicularly to the layers' plane and acting on F_1 and F_2 can be expressed as sums of their in-plane and out-of-plane components, $\boldsymbol{\tau}_1 = \boldsymbol{\tau}_{1\parallel} + \boldsymbol{\tau}_{1\perp}$ and $\boldsymbol{\tau}_2 = \boldsymbol{\tau}_{2\parallel} + \boldsymbol{\tau}_{2\perp}$, respectively. In the CFL structure, STT acting on the F_1 layer results from the polarizer F_0, as well as from the F_2 layer, while the STT acting on F_2 is due to the F_1 layer. Hence we can write

$$\boldsymbol{\tau}_{1\parallel} = I\hat{\mathbf{S}}_1 \times \left[\hat{\mathbf{S}}_1 \times \left(a_1^{(0)}\hat{\mathbf{S}}_0 + a_1^{(2)}\hat{\mathbf{S}}_2\right)\right], \quad (3a)$$
$$\boldsymbol{\tau}_{1\perp} = I\hat{\mathbf{S}}_1 \times \left(b_1^{(0)}\hat{\mathbf{S}}_0 + b_1^{(2)}\hat{\mathbf{S}}_2\right), \quad (3b)$$
$$\boldsymbol{\tau}_{2\parallel} = I a_2^{(1)}\,\hat{\mathbf{S}}_2 \times (\hat{\mathbf{S}}_2 \times \hat{\mathbf{S}}_1), \quad (3c)$$
$$\boldsymbol{\tau}_{2\perp} = I b_2^{(1)}\,\hat{\mathbf{S}}_2 \times \hat{\mathbf{S}}_1, \quad (3d)$$

where I is the charge current density, which is positive when electrons flow from the layer F_2 towards F_0 (see Fig. 1). The parameters $a_i^{(j)}$ and $b_i^{(j)}$ $(i,j = 1,2)$ are independent of current I, but generally depend on the magnetic configuration of the whole structure. Moreover, their magnitudes depend on the model of electronic transport. Here, we calculate them as a function of magnetic configuration in the regime of diffusive transport.[21,24]

Finally, we write the thickness of F_1 as $d_1 = \xi d$, where $d = d_2$. Then the interlayer exchange fields can be written as $H_{\mathrm{RKKY}\,2} = H_{\mathrm{RKKY}}$ and $H_{\mathrm{RKKY}\,1} = \xi^{-1}H_{\mathrm{RKKY}}$. In this paper we focus on $\xi > 1$.[21] Dynamical features of the opposite case ($\xi < 1$) have been studied in Refs. 28 and 29.

B. Linearized Landau-Lifshitz-Gilbert equation

In order to study stability of the static states we first write the two coupled equations (1) in the local coordinates defined by the base vectors $\hat{\boldsymbol{e}}_{\phi i} = (\hat{\boldsymbol{e}}_z \times \hat{\mathbf{S}}_i)/\sin\theta_i$ and $\hat{\boldsymbol{e}}_{\theta i} = \hat{\mathbf{S}}_i \times \hat{\boldsymbol{e}}_{\phi i}$, where $i = 1,2$ and θ_i is the angle between $\hat{\mathbf{S}}_i$ and $\hat{\boldsymbol{e}}_z$. In this coordinate system, configuration of the CFL can be described as a point in the four-dimensional space, $\tilde{\boldsymbol{S}} = (\theta_1,\phi_1,\theta_2,\phi_2)^{\intercal}$, and the LLG equation reads

$$\frac{d\tilde{\boldsymbol{S}}}{dt} = \bar{\boldsymbol{M}} \cdot \tilde{\boldsymbol{\omega}}, \quad (4)$$

where $\bar{\boldsymbol{M}}$ is the 4×4 block-diagonal matrix, $\bar{\boldsymbol{M}} = \left(\begin{smallmatrix} \boldsymbol{L}_1 & \mathbf{0} \\ \mathbf{0} & \boldsymbol{L}_2 \end{smallmatrix}\right)$, where

$$\boldsymbol{L}_i = \begin{pmatrix} 1 & \alpha \\ -\alpha/\sin\theta_i & 1/\sin\theta_i \end{pmatrix} \quad (5)$$

for $i = 1,2$. For simplicity, we assumed that the damping parameter is small, i.e., $\alpha^2 \ll 1$. Moreover, $\tilde{\boldsymbol{\omega}} = (\omega_{\theta 1},\omega_{\phi 1},\omega_{\theta 2},\omega_{\phi 2})^{\intercal}$, where $\omega_{\theta i} = \boldsymbol{\Gamma}_i \cdot \hat{\boldsymbol{e}}_{\theta i}$, and $\omega_{\phi i} = \boldsymbol{\Gamma}_i \cdot \hat{\boldsymbol{e}}_{\phi i}$. The point $\tilde{\boldsymbol{S}}_0 = (\theta_{01},\phi_{01},\theta_{02},\phi_{02})^{\intercal}$ is said to be static when $\omega_{\theta i} = 0$ and $\omega_{\phi i} = 0$ for $i = 1,2$, and hence $d\tilde{\boldsymbol{S}}_0/dt = 0$.

In order to study stability of the static points we shall linearize Eq. (4) in the vicinity of $\tilde{\boldsymbol{S}}_0$. The linearized LLG equation for the deviations from the static point, $\boldsymbol{\delta}\tilde{\boldsymbol{S}}(t) = \tilde{\boldsymbol{S}}(t) - \tilde{\boldsymbol{S}}_0$, can be then written as

$$\frac{d}{dt}\boldsymbol{\delta}\tilde{\boldsymbol{S}} = \bar{\boldsymbol{D}} \cdot \boldsymbol{\delta}\tilde{\boldsymbol{S}}, \quad (6)$$

where $\bar{\boldsymbol{D}}$ is the 4×4 dynamic matrix, calculated in the static point $\tilde{\boldsymbol{S}}_0$. This matrix can be written as $\bar{\boldsymbol{D}} = \bar{\boldsymbol{M}} \cdot \bar{\boldsymbol{J}}$, with $\bar{\boldsymbol{J}}$ being the 4×4 Jacobian matrix of elements $J_{ij} = \partial\tilde{\omega}_i/\partial\tilde{S}_j$. Structure of the matrix $\bar{\boldsymbol{D}}$ is given in Appendix A, where we assumed that the out-of-plane STT components were negligible in comparison to the in-plane ones and hence were disregarded.

C. Methods of stability analysis

In the following we shall focus on the stability of static points in the layers' plane. The CFL with antiferromagnetic coupling has two such points. Following Fig. 1, one of the static points of the CFL dynamics corresponds to the configuration

with $\hat{\boldsymbol{S}}_1 = -\hat{\boldsymbol{e}}_z$ and $\hat{\boldsymbol{S}}_2 = \hat{\boldsymbol{e}}_z$. In this configuration, $\hat{\boldsymbol{S}}_1$ is antiparallel to the fixed layer's spin $\hat{\boldsymbol{S}}_0$. Therefore, we shall call this configuration (static state) as an antiparallel (AP) one. The second static point of the CFL corresponds to $\hat{\boldsymbol{S}}_1 = \hat{\boldsymbol{e}}_z$ and $\hat{\boldsymbol{S}}_2 = -\hat{\boldsymbol{e}}_z$. This configuration will be referred to in the following as the parallel (P) one.

We shall investigate stability of these static points by analyzing signs of the eigenvalues of the dynamic matrix, using the Lyapunov method.[22] Then we will apply the Routh-Hurwitz criterion to study the critical current required for the current-induced excitation of the studied CFL.

1. Lyapunov method

Considering the linearized LLG Eq. (6) for $\delta\tilde{\boldsymbol{S}}(t)$, one can write the solution in the form $\delta\tilde{\boldsymbol{S}}(t) = \exp(\bar{\boldsymbol{D}}t)\,\delta\tilde{\boldsymbol{S}}_0$, where $\delta\tilde{\boldsymbol{S}}_0$ is the initial deviation of $\tilde{\boldsymbol{S}}$ from the equilibrium $\tilde{\boldsymbol{S}}_0$. The Lyapunov theorem says that the studied static state $\tilde{\boldsymbol{S}}_0$ is stable, if and only if all the eigenvalues of $\bar{\boldsymbol{D}}$ have negative real parts. If one of them becomes positive, the static point is unstable. More precisely, if all the eigenvalues have negative real parts we call the static point as *stable node*. Oppositely, when all of them are positive we talk about *unstable node*. If some of the eigenvalues have positive and some negative real parts, the static point is a *saddle point*.[22]

2. Routh-Hurwitz method

The Routh-Hurwitz theorem[23] allows one to decide when the eigenvalues of the dynamic matrix have negative real parts. Let us assume the characteristic polynomial of $\bar{\boldsymbol{D}}$, $P(\lambda) = \det(\bar{\boldsymbol{D}} - \lambda\bar{\boldsymbol{I}})$, where $\bar{\boldsymbol{I}}$ is the 4×4 unit matrix. $P(\lambda)$ is a fourth-order polynomial, which can be generally written as

$$P(\lambda) = \lambda^4 + c_3\lambda^3 + c_2\lambda^2 + c_1\lambda + c_0. \tag{7}$$

Now let us consider matrix of the form,

$$H_P = \begin{pmatrix} c_1 & c_0 & 0 & 0 \\ c_3 & c_2 & c_1 & c_0 \\ 0 & 1 & c_3 & c_2 \\ 0 & 0 & 0 & 1 \end{pmatrix}. \tag{8}$$

The Routh-Hurwitz theorem says that the eigenvalues λ of $\bar{\boldsymbol{D}}$ have negative real parts if and only if all the leading principal minors of H_P are positive. In other words, the considered static point is stable when the following inequalities are obeyed:

$$\Delta_1 = c_1 > 0, \tag{9a}$$

$$\Delta_2 = \det\begin{pmatrix} c_1 & c_0 \\ c_3 & c_2 \end{pmatrix} > 0, \tag{9b}$$

$$\Delta_3 = \det\begin{pmatrix} c_1 & c_0 & 0 \\ c_3 & c_2 & c_1 \\ 0 & 1 & c_3 \end{pmatrix} > 0. \tag{9c}$$

Since the fourth leading principal minor, Δ_4, is identical to the third one, Δ_3, the stability of a static state is described by the three conditions (9) in terms of the coefficients of the characteristic polynomial. The determinants Δ_i are also known as the *Hurwitz determinants*.

The coefficients c_i can be expressed in terms of the elements of dynamic matrix $\bar{\boldsymbol{D}}$, given in Appendix A. Thus, $c_0 = \det\{\bar{\boldsymbol{D}}\}$ and $c_3 = -\mathrm{Tr}\{\bar{\boldsymbol{D}}\}$. In turn, c_2 can be calculated as a sum of all 2×2 principal minors of $\bar{\boldsymbol{D}}$, while c_1 is equal to the minus sum of all 3×3 principal minors of $\bar{\boldsymbol{D}}$ (see, e.g., p. 196 in Ref. 30).

III. RESULTS

Let us now analyze the LLG equation, linearized in the static points. First, we will consider the AP static configuration ($\hat{\boldsymbol{S}}_1 = -\hat{\boldsymbol{S}}_2 = -\hat{\boldsymbol{e}}_z$), and at the end of this section we will analyze briefly the second static configuration, i.e., the P one. We start our considerations from the analysis of the eigenvalues of the matrix $\bar{\boldsymbol{D}}$ as a function of applied magnetic field and current density. Then, we shall study the signs of the Hurwitz determinants. Finally, we will analyze the critical current and compare the results with those obtained from numerical simulations.

In the numerical calculations of the spin transfer torque we assume the following structure, Cu–IrMn(10)/Py(8)/Cu(8)/Co(ξd)/Ru(1)/Co(d)–Cu, where the numbers in the brackets are layer thicknesses in nanometers. The electrodes and the first nonmagnetic spacer, N_0, are made of copper. As the antiferromagnetic layer we assume a 10-nm thick layer of IrMn. The polarizing layer is assumed to be made of 8 nm of permalloy (Py), while the CFL consists of cobalt films separated by a 1-nm thick layer of Ruthenium. Other parameters used in the simulations are $H_{\mathrm{ani}} = 0.56\,\mathrm{kOe}$ ($45\,\mathrm{kAm^{-1}}$) and $M_{\mathrm{s}} = 17.84\,\mathrm{kOe}$ ($1.42\,\mathrm{MAm^{-1}}$). The dominant components of the demagnetizing fields are $H^{\mathrm{d}}_{ix} \simeq M_{\mathrm{s}}$. The Gilbert damping parameter was as large as $\alpha = 0.01$. For zero and relatively small applied magnetic fields, smaller than the spin-flop fields, $H^{-}_{\mathrm{sf}} < H_{\mathrm{app}} < H^{+}_{\mathrm{sf}}$, the CFL remains antiparallel and aligned along the effective magnetic field in the absence of current.[27] We estimated numerically the spin-flop fields of the studied free layers to be close to $|H^{\pm}_{\mathrm{sf}}| \simeq 2.5\,\mathrm{kOe}$. To remain in this regime, we shall focus on the applied magnetic fields $|H_{\mathrm{app}}| \ll |H^{\pm}_{\mathrm{sf}}|$. Some other parameters used in simulations are given in Appendix B.

A. Antiparallel configuration

1. Eigenvalues of $\bar{\boldsymbol{D}}$ and Lyapunov analysis

Consider two CFL structures—a SyAF corresponding to $\xi = 1$, and a SyF corresponding $\xi = 2$. In both cases we assume $d = 2\,\mathrm{nm}$ for the thickness of the layer F_2, and $H_{\mathrm{RKKY}} = -2\,\mathrm{kOe}$ for the corresponding interlayer exchange field. The latter corresponds to $J_{\mathrm{RKKY}} \simeq -0.6\,\mathrm{mJ/m^2}$, which is close to experimentally measured values.[27,31] Figure 2 presents results of the stability analysis of the AP magnetic configuration of both CFL structures. The maps presenting signs of the eigenvalues of the matrix $\bar{\boldsymbol{D}}$ are shown as a function of the applied magnetic field, H_{app}, and current density I. These maps are divided into several regions. In both cases, (i) labels the regions where all eigenvalues of $\bar{\boldsymbol{D}}$ have negative real parts and hence the AP configuration is a stable node. In contrast, the regions (ii) and (iii) cover the values of H_{app} and I, where the AP configuration is unstable. In the regions (ii) the studied static point is a saddle point with two of the eigenvalues having positive and two negative real parts. In turn,

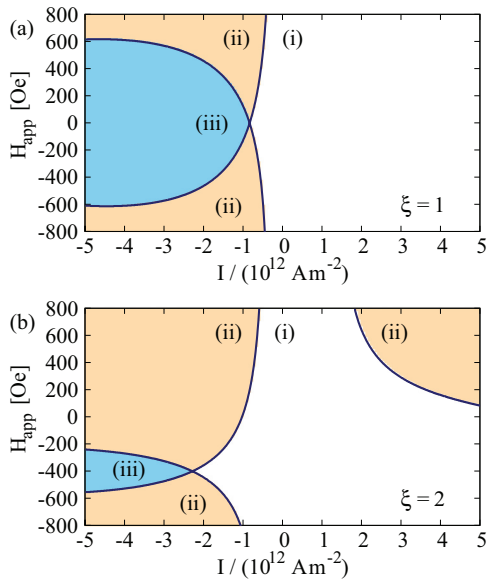

FIG. 2. (Color online) Maps presenting signs of the eigenvalues of the dynamic matrix in the AP configuration for a CFL with (a) $\xi = 1$ (SyAF) and (b) $\xi = 2$ (SyF). In the calculations we assumed $d = 2$ nm and $H_{\mathrm{RKKY}} = -2$ kOe. All the eigenvalues have negative real parts in the areas marked as (i). Two eigenvalues have positive real parts in the areas (ii), while in the regions (iii) all the eigenvalues have positive real parts. The other parameters as described in the text.

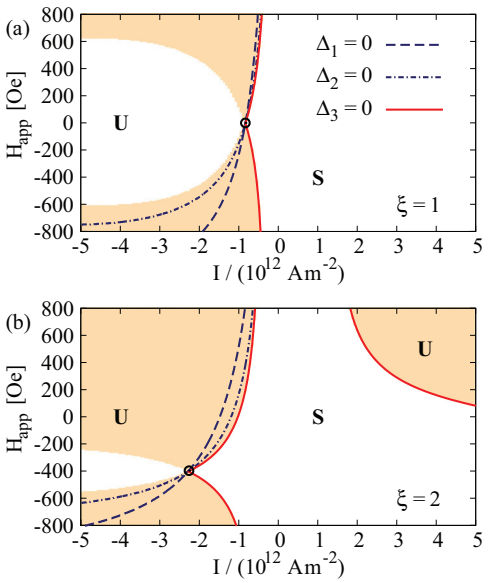

FIG. 3. (Color online) Maps of the signs of Hurwitz determinants in the AP configuration for CFL with (a) $\xi = 1$ (SyAF) and (b) $\xi = 2$ (SyF). The other parameters are the same as in Fig. 2. The stable (S) and unstable (U) regions are separated by the red (solid) lines, which correspond to the critical current densities. The color (dark) areas cover the range of parameters where $\Delta_3 < 0$. The dashed and dot-dashed lines correspond to $\Delta_1 = 0$ and $\Delta_2 = 0$, respectively.

in the regions (iii) the AP configuration becomes an unstable node since all the eigenvalues have positive real parts.

In both cases the CFL dynamics is excited for negative currents. In the case of SyF, an unstable region appears also for $I > 0$ and $H_{\mathrm{app}} > 0$, as one can see in Fig. 2(b). An important feature of the diagrams in Fig. 2 is a nonmonotonous variation of the boundary between the stable and unstable regions with H_{app}. This boundary corresponds to the critical current density, $I_c^{\mathrm{AP}}(H_{\mathrm{app}})$, needed to destabilize the AP configuration at a given value of H_{app}. Now we shall analyze the AP state in more detail, using the Routh-Hurwitz formulation of the local stability.

2. *Hurwitz determinants*

Figure 3 depicts signs of the Hurwitz determinants, Δ_i ($i = 1,2,3$), as a function of I and H_{app} in the AP configuration and for the same parameters as in Fig. 2. The stable (S) and unstable (U) regions are separated by the red (solid) lines. Moreover, the dashed and dot-dashed lines correspond to the points where Δ_1 and Δ_2 change sign, i.e., they correspond to the solutions of $\Delta_1 = 0$ and $\Delta_2 = 0$, respectively. Finally, the color (dark) areas correspond to negative Δ_3; elsewhere Δ_3 is positive. Two important features of the diagrams can be noticed immediately. First, the areas with $\Delta_3 < 0$ coincide exactly with the areas, where the AP static point is a saddle point, i.e., with the regions marked as (ii) in Fig. 2. Moreover, when increasing the current density (either in the positive or negative direction), Δ_3 is the first of the three Hurwitz determinants which becomes negative at a given H_{app}. Hence, its sign determines stability of the AP state, and the whole information about the critical current density can be obtained from solution of $\Delta_3 = 0$. Second, from the numerical calculations it seems that all the three curves corresponding to sign change of the corresponding Hurwitz determinants intersect at one point marked with the circle on the diagrams. In the following, the current density in the AP configuration corresponding to this point will be denoted as I_0^{AP}, and the corresponding applied magnetic field as H_0^{AP}. The negative critical current reaches maximum at the intersection point. In our previous numerical study we have shown that this point is important for the description of the current-induced dynamics of a CFL.[21] Therefore, we shall study it in more detail.

Let us consider the intersection point of the curves determined by $\Delta_1 = 0$ and $\Delta_2 = 0$. The first equation gives $c_1 = 0$, while from the second one follows that $c_0 c_3 = 0$, i.e., either $c_0 = 0$ or $c_3 = 0$. When $c_1 = 0$, the third Hurwitz determinant is $\Delta_3 = -c_0 c_3^2$, which vanishes in the considered points of intersection. This proves that all three lines given by $\Delta_i = 0$ ($i = 1,2,3$) intersect in the same point obeying either $c_1 = c_0 = 0$ or $c_1 = c_3 = 0$. Moreover, taking the first derivatives of $\Delta_3 = \Delta_3(I, H_{\mathrm{app}})$, one can see that $\partial\Delta_3/\partial I = \partial\Delta_3/\partial H_{\mathrm{app}} = 0$ when $c_1 = c_3 = 0$. This means that this intersection represents a double point of the curve given by $\Delta_3 = 0$ (see, e.g., Ref. 32). Depending on the second derivatives of Δ_3, this point may be either a node or a cusp. In Fig. 3, this intersection corresponds to I_0^{AP} and H_0^{AP}. On the other hand the first derivatives of Δ_3 do not generally vanish in the point given by $c_1 = c_0 = 0$, which rules out the existence of a double point there. These results fully agree with numerical evaluation of the Hurwitz determinants and are independent on the form of effective magnetic field and STT.

3. Critical currents

Let us now make use of the above observations and derive the formula for the maximum critical current density given by the intersection point of the curves defined by $\Delta_i = 0$ ($i = 1,2,3$) and corresponding to the conditions $c_1 = c_3 = 0$. From the equation $c_3 = 0$ one can obtain a simple solution for the maximum critical current density in the form,

$$I_0^{\mathrm{AP}} = -\alpha \frac{\mu_0 M_s \xi d}{a_1^{(0)} + a_1^{(2)} + \xi a_2^{(1)}} \times \left[2 H_{\mathrm{ani}} + H_1^{\mathrm{d}} + H_2^{\mathrm{d}} - (1+\xi^{-1}) H_{\mathrm{RKKY}}\right], \quad (10)$$

where $H_i^{\mathrm{d}} = (H_{ix}^{\mathrm{d}} + H_{iy}^{\mathrm{d}})/2 - H_{iz}^{\mathrm{d}}$, and the parameters $a_i^{(j)}$ correspond to the AP configuration. Note, equation $c_3 = 0$ is equivalent to $\mathrm{Tr}\{\bar{\boldsymbol{D}}\} = 0$, used to derive Eq. (12) in Ref. 21. Moreover, the condition $c_0 = 0$, equivalent to $\det\{\bar{\boldsymbol{D}}\} = 0$, also determines intersection points of $\Delta_i = 0$. This condition leads to a fourth-order equation for the current density with the corresponding coefficients dependent on the applied magnetic field. However, c_0 has no real roots in the range of H_{app} under consideration. Substituting Eq. (10) into the equation $\Delta_1 = 0$ one obtains a quadratic equation for H_0^{AP}, with one solution being in the range of interest. Since the analytical expression for H_0^{AP} is cumbersome, we shall study it only numerically.

Figures 4(a)–4(d) show variation of I_0^{AP} and H_0^{AP} with the magnitude of H_{RKKY} and ξ. Note that when varying ξ at constant d, one has to change the thickness of the layer F_1, and consequently also its demagnetization field. In addition, the torque parameters $a_i^{(j)}$ also depend on the layer's thicknesses. Since these quantities are obtained from independent numerical calculations, we evaluated them for several pillar structures and fitted them as linear functions of ξ. In Fig. 4(a), the linear dependence of I_0^{AP} on H_{RKKY} is shown for several values of ξ ranging from $\xi = 1$ to $\xi = 2$. Magnitude of the critical current density, $|I_0^{\mathrm{AP}}|$, increases with increasing magnitude of the interlayer exchange field, $|H_{\mathrm{RKKY}}|$. Moreover, $|I_0^{\mathrm{AP}}|$ increases with increasing CFL asymmetry (increasing ξ). The slope of $I_0^{\mathrm{AP}}(H_{\mathrm{RKKY}})$ only slightly changes with ξ. The increase of $|I_0^{\mathrm{AP}}|$ with ξ is systematically shown in Fig. 4(b) for $H_{\mathrm{RKKY}} = -1$, -2, and -3 kOe. It can be noticed that I_0^{AP} depends rather weakly on the RKKY coupling field. Figure 4(c) shows H_0^{AP} as a function of H_{RKKY}. In the case of SyAF ($\xi = 1$), H_0^{AP} is rather independent of H_{RKKY} and $H_0^{\mathrm{AP}} \simeq 0$. For SyF ($\xi > 1$), H_0^{AP} changes linearly with H_{RKKY}, and the slope of this linear dependence strongly increases with increasing ξ. Finally, Fig. 4(d) shows the variation of H_0^{AP} with ξ. Similarly to $|I_0^{\mathrm{AP}}|$, H_0^{AP} in the SyF free layers is shifted towards higher absolute values with increasing ξ. This trend is even more pronounced when the magnitude of interlayer exchange coupling is stronger. In addition, the circles in Fig. 4 correspond to the results of numerical macrospin simulations based on the LLG equations with the in-plane and out-of-plane STT included, as described by Eq. (1). In Figs. 4(a) and 4(c) we compare the analytical results with numerical simulations for the SyF free layer with $\xi = 1.25$ and H_{RKKY} ranging from -1 to -3 kOe. In turn, in Figs. 4(b) and 4(d) we show the results of simulations for $H_{\mathrm{RKKY}} = -2$ kOe, and ξ varying from 1 to 2.25. A good agreement of the analytical results with those obtained from model macrospin simulations is evident.

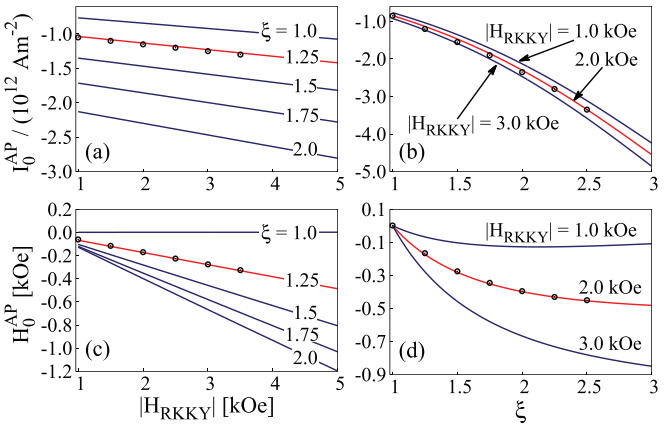

FIG. 4. (Color online) The dependence of I_0^{AP} (a) and H_0^{AP} (c) on the magnitude of H_{RKKY} for indicated values of ξ. The circles present the results of numerical simulations for $\xi = 1.25$. (b) and (d) The dependence of I_0^{AP} and H_0^{AP} on ξ for various values of H_{RKKY}. The circles show the results of numerical simulations for $|H_{\mathrm{RKKY}}| = 2$ kOe. All results are for $d = 2$ nm and other parameters as in Fig. 2.

Consider now the critical current I_c^{AP} in the whole considered range of the applied magnetic fields H_{app}. This critical current can be obtained from solution of the equation $\Delta_3 = 0$, which is a sixth-order equation in I. Here, we restrict ourselves to the solutions which are real in the whole range of magnetic field under consideration. These solutions correspond to the red (solid) lines in Figs. 3(a) and 3(b) for the SAF and SyF free layers, respectively. The variation of $I_c^{\mathrm{AP}}(H_{\mathrm{app}})$ with ξ is shown in more detail in Fig. 5(a). One can note a systematical shift in the amplitude of the critical current with increasing ξ. The inset in Fig. 5(a) shows the positive branch of the solution for critical current. When the CFL asymmetry increases (increasing ξ), the positive unstable region is shifted towards lower values of the current density and applied magnetic field. The direct comparison of the numerical simulations based on the LLG equation with the results derived from the analytical model is shown in Fig. 5(b). The simulations were performed as follows. We started from a configuration, where the free layer's spins were tilted by 1° from the AP configuration. Initially, for given values of H_{app} and I, we solved numerically Eq. (1) for 50 ns of the simulated dynamics, until the system reached its equilibrium. Then, for the next 30 ns we were collecting the data for averaging. The time-averaged resistance of the spin valve R is shown on the map in Fig. 5(b). The largest values of R correspond to the AP magnetic configuration. When the current amplitude exceeds the critical value, the CFL either switches to another static state, or remains in a steady-state dynamic mode. In both cases there is a drop in the average resistance. For more details on the numerical simulations we refer to Ref. 21. The dashed line in Fig. 5(b) corresponds to the results based on the linearized LLG equation and the stability analysis. This figure shows a very good agreement of the model calculations with the macrospin numerical simulations. Some small deviations may be attributed to neglecting the out-of-plane torque components

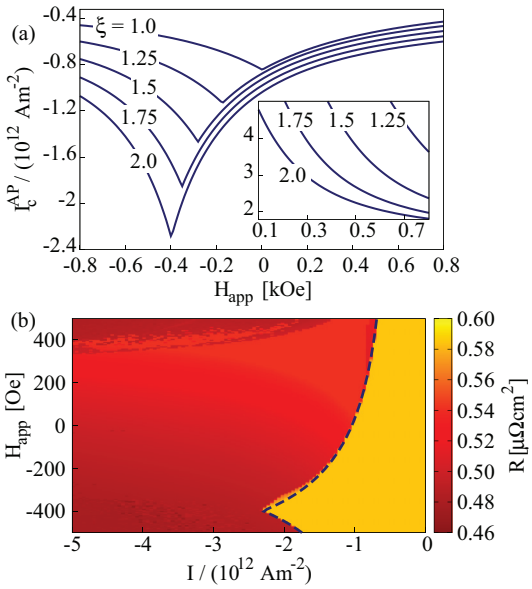

FIG. 5. (Color online) (a) Critical current density in the AP configuration, as a function of applied magnetic field for CFLs corresponding to indicated values of ξ. (b) Direct comparison of the numerical macrospin simulations and the analytical model for the SyF free layer with $\xi = 2$, $d = 2$ nm, and $H_{RKKY} = -2$ kOe. The resistance of spin valve after 30 ns of the current-induced dynamics is shown in the color (gray) scale. The dashed line corresponds to the analytical result derived from the model calculations. The other parameters as in Fig. 2.

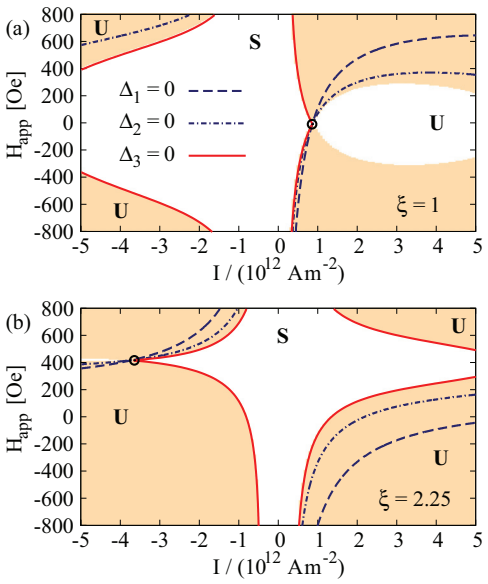

FIG. 6. (Color online) Map of the signs of Hurwitz determinants in the P configuration for CFL with (a) $\xi = 1$ (SyAF) and (b) $\xi = 2.25$ (SyF). Other parameters are the same as in Fig. 2. The stable (S) and unstable (U) regions are separated by the red (solid) lines which correspond to the critical current. The color (gray) areas cover the range of parameters where $\Delta_3 < 0$. The dashed and dot-dashed lines correspond to the solutions of $\Delta_1 = 0$ and $\Delta_2 = 0$, respectively. The other parameters are as in Fig. 2.

in the linearized LLG equation, and/or to nonlinearities of the LLG equation.

In addition, using the tangents of $\Delta_3 = 0$ in the vicinity of the double point, the critical current line can be approximated at this point as $I_{0\pm}^{AP} = I_0^{AP} + K_\pm (H_0^{AP} - H_{app})$, where

$$K_\pm = \frac{q c_2 - 2c_1' \pm q\sqrt{c_2^2 - 4c_0^2}}{2[(c_1')^2 - q c_2 c_1' + c_0 q^2]} \frac{\partial c_1}{\partial H_{app}}, \qquad (11)$$

with $c_1' = \partial c_1/\partial I$. Here, we already took into account that c_3 is independent on H_{app}, and $q = 2\gamma_g (a_1^{(0)} + a_1^{(2)} + \xi a_2^{(1)})/(M_s \xi d)$.

B. Parallel configuration

Consider now the second static state of the CFL, i.e., the parallel configuration, $\hat{\boldsymbol{S}}_1 = -\hat{\boldsymbol{S}}_2 = \hat{\boldsymbol{e}}_z$. Figure 6 shows the maps of the signs of the three Hurwitz determinants in the P configuration for SyAF (a) and for SyF corresponding to $\xi = 2.25$ (b). All the other parameters are the same as in Fig. 3. Similarly as in the case of AP configuration, there is a point, where all the three lines determined by $\Delta_i = 0$ ($i = 1,2,3$) intersect. Critical current corresponding to this point will be denoted as I_0^P and the corresponding magnetic field as H_0^P. For the SyAF free layer, I_0^P is the maximum positive critical current. However, apart from the positive branch of critical current (including the I_0^P point), there is another real solution of $\Delta_3 = 0$ for negative values of I. Moreover, I_0^P becomes negative in the case of a SyF free layer. To elucidate the change of I_0^P sign, we first derive the corresponding formula in the same way as in the case of AP configuration. As a result we find

$$I_0^P = \alpha \frac{\mu_0 M_s \xi d}{a_1^{(0)} - a_1^{(2)} - \xi a_2^{(1)}} \times \left[2 H_{ani} + H_1^d + H_2^d - (1 + \xi^{-1}) H_{RKKY}\right], \qquad (12)$$

where $a_i^{(j)}$ are taken now in the P configuration. Analyzing Eq. (12) one finds that I_0^P changes sign at the point where the corresponding denominator becomes zero. Hence, the critical value of ξ, $\xi = \xi_c$, at which the critical current changes sign is given by the equation,

$$a_1^{(0)}(\xi_c) - a_1^{(2)}(\xi_c) - \xi_c a_2^{(1)}(\xi_c) = 0. \qquad (13)$$

Taking into account the linear dependence of $a_i^{(j)}$ on ξ, Eq. (13) becomes a quadratic equation with the relevant solution for the studied CFL structures, $\xi_c \simeq 1.85$. Such a critical value of ξ, where critical current changes sign, does not appear in the AP configuration, since the denominator of (10) does not vanish for any real value of the parameter ξ.

Figure 7(a) shows the dependence of I_0^P on $|H_{RKKY}|$ for several values of ξ. The three top lines were calculated for $\xi < \xi_c$, and hence $I_0^P > 0$. The magnitude of I_0^P slightly increases with the interlayer coupling and also with increasing ξ. For $\xi > \xi_c$ we obtain negative I_0^P in the whole range of the studied values of H_{RKKY}. The absolute magnitude of critical current density increases then with increasing H_{RKKY} and diminishes with increasing ξ. Variation of the critical current with ξ is shown in Fig. 7(b). I_0^P initially increases with increasing ξ, until ξ passes the critical value, at which the current changes sign to negative and then it increases towards $I_0^P = 0$. Note

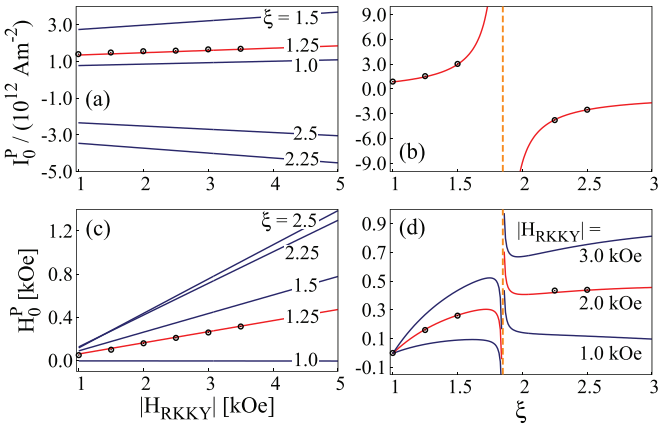

FIG. 7. (Color online) (a) and (c) The dependence of I_0^{P} and H_0^{P} on the magnitude of H_{RKKY} for various values of ξ. The circles show the results of numerical simulations for $\xi = 1.25$. (b) and (d) The dependence of I_0^{P} and H_0^{P} on ξ for various values of H_{RKKY}. In (b) only the curve for $|H_{\mathrm{RKKY}}| = 2$ kOe is shown as the other two are very close. The circles show the results of numerical simulations for $|H_{\mathrm{RKKY}}| = 2$ kOe. The vertical line corresponds to the critical value of ξ, $\xi_c \simeq 1.85$. All results are for $d = 2$ nm and the other parameters are as in Fig. 2.

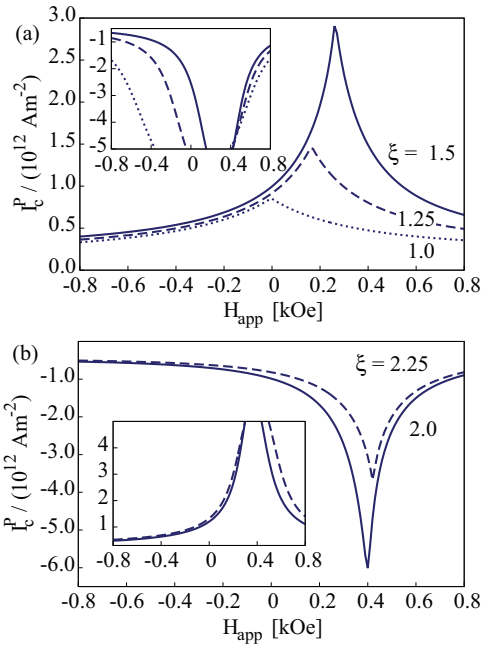

FIG. 8. (Color online) Critical current density in the P configuration as a function of the applied magnetic field, calculated for CFLs with (a) $\xi < \xi_c$ and (b) $\xi > \xi_c$. The results are for $H_{\mathrm{RKKY}} = -2$ kOe and $d = 2$ nm, and the other parameters are as in Fig. 2.

that Fig. 7(b) shows the curve for $H_{\mathrm{RKKY}} = -2$ kOe since the curves calculated for $H_{\mathrm{RKKY}} = -1$ and -3 kOe are very close. Magnitude of the corresponding applied magnetic field, H_0^{P}, is shown in Fig. 7(c) as a function of H_{RKKY}. For all considered values of ξ, we find linear increase of H_0^{P} with the coupling strength. Figure 7(d) shows H_0^{P} as a function of ξ. One can see that the magnitude of H_0^{P} initially increases and then abruptly falls down in the vicinity of $\xi = \xi_c$. Above the critical value ξ_c, H_0^{P} varies rather slowly with increasing ξ. As before, the points marked by the circles were obtained from numerical simulations. Similarly as in the AP configuration, a very good agreement of the model calculations based on the linearized LLG equation and numerical simulations has been achieved.

Finally, Fig. 8 shows the critical current I_c^{P} in the P configuration as a function of H_{app}. The case of $\xi < \xi_c$ is shown in Fig. 8(a), where the curves clearly show the shift of I_0^{P} with ξ and also increase in I_c^{P} with increasing ξ. The inset to this figure shows the solution for critical current on the negative current side, $I < 0$. In contrast, Fig. 8(b) depicts critical currents for $\xi > \xi_c$. These results clearly show a reduction of I_c^{P}, and also of I_0^{P}, at higher values of ξ (when it exceeds ξ_c). The branch for positive I_c^{P} is shown in the inset.

As in the AP configuration, the critical current near the double point can be expressed by Eq. (11) with $q = -2\,\gamma_g\,(a_1^{(0)} - a_1^{(2)} - \xi\, a_2^{(1)})/(M_s\,\xi\, d)$. As one can note, both tangents become identical when $\xi = \xi_c$.

IV. SUMMARY AND CONCLUSIONS

We have carried out a stability analysis of the in-plane static configurations of a spin valve composed of polarizer and composite free layer with antiferromagnetic interlayer exchange coupling. The approach was based on the linearized Landau-Lifshitz-Gilbert equation. Employing the Routh-Hurwitz theorem we have described the critical current density for the current-induced dynamic excitations. A satisfactory agreement between the presented analytical model and numerical simulations in the macrospin approximation has been achieved. This agreement indicates a minor importance of the out-of-plane torque components, which were disregarded in the linearized model but were included in the numerical simulations—similarly as in the case of a single spin stability, where the out-of-plane components enter the expression for critical current *via* a term proportional to the (small) Gilbert damping constant.[13]

In particular, we have shown that the complete information about the critical current density in the studied range of applied magnetic field, H_{app}, is given by the roots of the third Hurwitz determinant, $\Delta_3 = 0$. This, however, might change at stronger magnetic fields, close to the spin-flop phase, where Δ_1 or Δ_2 might become negative at smaller current densities than Δ_3 does. In such a case, the condition $\Delta_1 = 0$ or $\Delta_2 = 0$ would yield the critical current at a given H_{app}.

For both studied magnetic configurations (static states), we have derived analytical expressions for the critical current density at the points given by condition $c_1 = c_3 = 0$, where the roots of all three Hurwitz determinants intersect. We have shown that this point is a double point of the curve described by $\Delta_3 = 0$, which appears as a cusp on the critical current line. Near the double point, the critical current density can be approximated by a second-order curve. It can be shown that I_0^{AP} and I_0^{P} are simply related via the spin torque amplitudes as

$$\frac{I_0^{\mathrm{P}}}{I_0^{\mathrm{AP}}} = -\frac{a_1^{(0)}[\mathrm{AP}] + a_1^{(2)}[\mathrm{AP}] + \xi\, a_2^{(1)}[\mathrm{AP}]}{a_1^{(0)}[\mathrm{P}] - a_1^{(2)}[\mathrm{P}] - \xi\, a_2^{(1)}[\mathrm{P}]}. \qquad (14)$$

In our previous numerical study[21] of the current-induced dynamics of CFL structures, we have shown that the expressions for I_0^{AP} and I_0^{P} give maximum values of the current density required to observe current-induced reversal of the CFL in the AP and P configurations, respectively. Therefore, they may be useful in optimizing the CFL structures, in order to obtain current-induced switching at low current densities. It also has been shown that the sign of I_0^{P} can be changed by manipulating relative thicknesses of the two components of the CFL.

In addition, a frequently used approximation in composite layers is based on neglecting STT acting at the internal interfaces of CFL. Indeed, the magnitudes of internal STT components are smaller than the STT components due to the fixed layer. However, depending on the current direction, the internal STT components may stabilize or destabilize the relative magnetic configuration of the CFL, and therefore can influence the critical current. To evaluate the impact of internal STT components, one can, for instance, consider Eq. (10) for the critical current in the AP configuration at the cusp point. Neglecting the STT components acting on the internal interface of the F_1 layer (proportional to $a_1^{(2)}$), and taking calculated values of the parameters $a_1^{(2)}, a_1^{(0)}$, and $a_2^{(1)}$, one finds $\propto 18\%$ reduction of the critical current when $\xi = 1$, which is quite a significant amount.

In the presented stability analysis we have disregarded the interlayer magnetostatic interaction. This interaction can be easily included into the effective field in the form of generalized demagnetizing tensors.[26] From comparison with Ref. 21, one can conclude that the magnetostatic coupling does not change qualitatively the presented results, and gives rise to a shift of the critical current lines, mainly H_0^{AP} (H_0^{P}). Note, that neglecting the magnetostatic interactions might have a more serious influence on the CFL magnetization dynamics, which, however, was not studied in this paper.

ACKNOWLEDGMENT

This work has been carried out within Project No. NANOSPIN PSPB-045/2010 supported by a grant from Switzerland through the Swiss Contribution to the enlarged European Union. J.B. also acknowledges support from National Science Center in Poland as Project No. DEC-2012/04/A/ST3/00372.

APPENDIX A: DYNAMIC MATRIX

In this paper we focused on the study of static points in the layers' plane. To avoid the singularities of the chosen coordinate system at $\theta_1 = 0$ and $\theta_2 = 0$, we rotate the device so that the $\hat{\boldsymbol{e}}_z$ axis is perpendicular to the layer's plane. The in-plane static points of the dynamics are then located at $\theta_1 = \theta_2 = \pi/2$, and the static point marked as AP is given by $\phi_1 = 0$ and $\phi_2 = \pi$, while the static point P is located at $\phi_1 = \pi$ and $\phi_2 = 0$.

Evaluating $\bar{\boldsymbol{M}}$ and $\bar{\boldsymbol{J}}$ for $\theta_1 = \theta_2 = \pi/2$, one obtains the dynamic matrix which can be written in the block form $\bar{\boldsymbol{D}} = \left(\begin{smallmatrix} \boldsymbol{D}_1 & \boldsymbol{C}_{12} \\ \boldsymbol{C}_{21} & \boldsymbol{D}_2 \end{smallmatrix}\right)$, where $\boldsymbol{D}_i$ is the *single spin* dynamic matrix,

$$\boldsymbol{D}_i = \begin{pmatrix} \omega_i^{\tau} - \alpha\omega_i^{h1} & \alpha\omega_i^{\tau} - \omega_i^{h2} \\ -\alpha\omega_i^{\tau} - \omega_i^{h1} & \omega_i^{\tau} + \alpha\omega_i^{h2} \end{pmatrix}, \tag{A1}$$

and $\boldsymbol{C}_{ij}$ express the coupling between the free layer's spins,

$$\boldsymbol{C}_{ij} = \begin{pmatrix} -\omega_{ij}^{\tau} + \alpha\,\omega_{Ji} & -(\alpha\omega_{ij}^{\tau} + \omega_{Ji})\cos\Delta\phi \\ \alpha\omega_{ij}^{\tau} + \omega_{Ji} & -(\omega_{ij}^{\tau} - \alpha\omega_{Ji})\cos\Delta\phi \end{pmatrix}. \tag{A2}$$

In the latter expressions, the contribution due to effective field is included in ω_i^{h1} and ω_i^{h2}, which read

$$\begin{aligned} \omega_i^{h1} = {} & |\gamma_{\mathrm{g}}|\mu_0\big[\big(H_{\mathrm{ani}} - H_{iz}^{\mathrm{d}}\big)\cos^2\phi_i + H_{ix}^{\mathrm{d}} \\ & - H_{iy}^{\mathrm{d}}\sin^2\phi_i - H_{\mathrm{app}}\cos\phi_i\big] + \omega_{Ji}\cos\Delta\phi, \end{aligned} \tag{A3a}$$

$$\begin{aligned} \omega_i^{h2} = {} & |\gamma_{\mathrm{g}}|\mu_0\big[\big(H_{\mathrm{ani}} + H_{iy}^{\mathrm{d}} - H_{iz}^{\mathrm{d}}\big)\cos 2\phi_i \\ & + H_{\mathrm{app}}\cos\phi_i\big] - \omega_{Ji}\cos\Delta\phi, \end{aligned} \tag{A3b}$$

with $\Delta\phi = \phi_1 - \phi_2$, and $\omega_{J1} = \omega_J/\xi$ and $\omega_{J2} = \omega_J$, where

$$\omega_J = |\gamma_{\mathrm{g}}|\mu_0\, H_{\mathrm{RKKY}} = -\frac{|\gamma_{\mathrm{g}}|}{M_{\mathrm{s}}d}\, J_{\mathrm{RKKY}}. \tag{A4}$$

The spin torque contribution is given by ω_i^{τ} and ω_{ij}^{τ}, where

$$\omega_1^{\tau} = -\omega_{10}^{\tau}\cos\phi_1 + \omega_{12}^{\tau}\cos\Delta\phi, \tag{A5a}$$

$$\omega_2^{\tau} = \omega_{21}^{\tau}\cos\Delta\phi, \tag{A5b}$$

and

$$\omega_{ij}^{\tau} = \frac{a_i^{(j)} I}{\mu_0 M_{\mathrm{s}} d_i}. \tag{A6}$$

APPENDIX B: PARAMETERS USED IN NUMERICAL CALCULATIONS

Using the generalized demagnetizing tensor formalism[26] we calculated the demagnetization field of the free layers with elliptical cross section and with the major and minor axes

TABLE I. Bulk material parameters used for the layers.

Material	ρ^* ($\mu\Omega$cm)	β	λ_{sf} (nm)
Co	5.1	0.51	60
Py	16	0.77	5.5
Cu	0.5	0	350
Ru	9.5	0	14
IrMn	150	0	2

TABLE II. Interface material parameters used for the interfaces. The mixing conductance is given in $1/\mathrm{f}\Omega\mathrm{m}^2$.

Interface	R^* (fΩm^2)	γ	Re $G_{\uparrow\downarrow}$	Im $G_{\uparrow\downarrow}$
IrMn/Co	0.5	0.7	–	–
Co/Py	0.5	0.7	0.390	0.012
Co/Cu	0.5	0.77	0.542	0.016
Co/Ru	0.5	−0.2	0.260	0.008

of 130 and 60 nanometers, respectively. The elements of the demagnetization field have been fitted as a function of the layer's width, where d_i is given in nanometers,

$$H_{ix}^{\mathrm{d}} = (0.973 - 0.027\, d_i) M_{\mathrm{s}}, \tag{B1a}$$

$$H_{iy}^{\mathrm{d}} = (0.019 + 0.019\, d_i) M_{\mathrm{s}}, \tag{B1b}$$

$$H_{iz}^{\mathrm{d}} = (0.008 + 0.007\, d_i) M_{\mathrm{s}}. \tag{B1c}$$

The spin transfer torque, calculated in the frame of the diffusive transport model,[13,24] was evaluated for the material bulk and interfacial parameters given in Tables I and II, respectively.[13] In the tables, ρ^* describes the bulk resistivity, β is the bulk spin asymmetry parameter, and λ_{sf} is the spin diffusion length. The interface resistance is described by R^*, and γ the interface spin asymmetry factor. $G_{\uparrow\downarrow}$ stands for the mixing conductance, which is a complex number in general.

*balaz@ifmpan.poznan.pl

[1] T. L. Gilbert, IEEE Trans. Magn. **40**, 3443 (2004).
[2] J. C. Slonczewski, J. Magn. Magn. Mater. **159**, L1 (1996).
[3] L. Berger, Phys. Rev. B **54**, 9353 (1996).
[4] M. Tsoi, A. G. M. Jansen, J. Bass, W.-C. Chiang, M. Seck, V. Tsoi, and P. Wyder, Phys. Rev. Lett. **80**, 4281 (1998).
[5] J. A. Katine, F. J. Albert, R. A. Buhrman, E. B. Myers, and D. C. Ralph, Phys. Rev. Lett. **84**, 3149 (2000).
[6] J. Z. Sun, Phys. Rev. B **62**, 570 (2000).
[7] M. Gmitra and J. Barnaś, Appl. Phys. Lett. **89**, 223121 (2006).
[8] M. Gmitra and J. Barnaś, Phys. Rev. Lett. **96**, 207205 (2006).
[9] P. Ogrodnik, M. Wilczyński, R. Świrkowicz, and J. Barnaś, Phys. Rev. B **82**, 134412 (2010).
[10] Y. B. Bazaliy, B. A. Jones, and S.-C. Zhang, Phys. Rev. B **69**, 094421 (2004).
[11] U. Ebels, D. Houssameddine, I. Firastrau, D. Gusakova, C. Thirion, B. Dieny, and L. D. Buda-Prejbeanu, Phys. Rev. B **78**, 024436 (2008).
[12] I. Sodemann and Y. B. Bazaliy, Phys. Rev. B **84**, 064422 (2011).
[13] M. Gmitra and J. Barnaś, in *Toward Functional Nanomaterials*, edited by Z. Wang (Springer, New York, 2009), pp. 285–322.
[14] P. Grünberg, R. Schreiber, Y. Pang, M. B. Brodsky, and H. Sowers, Phys. Rev. Lett. **57**, 2442 (1986).
[15] S. S. P. Parkin and D. Mauri, Phys. Rev. B **44**, 7131 (1991).
[16] T. Ochiai, Y. Jiang, A. Hirohata, N. Tezuka, S. Sugimoto, and K. Inomata, Appl. Phys. Lett. **86**, 242506 (2005).
[17] D. Markó, T. Devolder, K. Miura, K. Ito, J.-V. Kim, C. Chappert, S. Ikeda, and H. Ohno, J. Appl. Phys. **112**, 053922 (2012).
[18] C.-Y. You, J. Appl. Phys. **107**, 073911 (2010).
[19] M. Ichimura, T. Hamada, H. Imamura, S. Takahashi, and S. Maekawa, J. Appl. Phys. **105**, 07D120 (2009).
[20] T. Devolder and K. Ito, J. Appl. Phys. **111**, 123914 (2012).
[21] P. Baláž and J. Barnaś, Phys. Rev. B **83**, 104422 (2011).
[22] S. Wiggins, *Introduction to Applied Nonlinear Dynamical Systems and Chaos* (Springer-Verlag, Berlin, 1990).
[23] F. R. Gantmacher, *Applications of the Theory of Matrices* (Wiley, New York, 1959).
[24] J. Barnaś, A. Fert, M. Gmitra, I. Weymann, and V. K. Dugaev, Phys. Rev. B **72**, 024426 (2005).
[25] W. H. Meiklejohn and C. P. Bean, Phys. Rev. **105**, 904 (1957).
[26] A. J. Newell, W. Williams, and D. J. Dunlop, J. Geophys. Res. **98**, 9551 (1993).
[27] D. Gusakova, D. Houssameddine, U. Ebels, B. Dieny, L. Buda-Prejbeanu, M. C. Cyrille, and B. Delaët, Phys. Rev. B **79**, 104406 (2009).
[28] C. Yoshida, Y. M. Lee, T. Ochiai, Y. Uehara, and T. Sugii, Appl. Phys. Lett. **99**, 222505 (2011).
[29] C. Klein, C. Petitjean, and X. Waintal, Phys. Rev. Lett. **108**, 086601 (2012).
[30] N. Jacobson, *Basic Algebra I.* (W. H. Freeman and Company, New York, 1986).
[31] D. Houssameddine, J. F. Sierra, D. Gusakova, B. Delaet, U. Ebels, L. D. Buda-Prejbeanu, M.-C. Cyrille, B. Dieny, B. Ocker, J. Langer, and W. Maas, Appl. Phys. Lett. **96**, 072511 (2010).
[32] H. Hilton, *Plane Algebraic Curves* (Oxford University Press, Oxford, 1932).